



AMERICAN METEOROLOGICAL SOCIETY

Journal of Climate

EARLY ONLINE RELEASE

This is a preliminary PDF of the author-produced manuscript that has been peer-reviewed and accepted for publication. Since it is being posted so soon after acceptance, it has not yet been copyedited, formatted, or processed by AMS Publications. This preliminary version of the manuscript may be downloaded, distributed, and cited, but please be aware that there will be visual differences and possibly some content differences between this version and the final published version.

The DOI for this manuscript is doi: 10.1175/JCLI-D-12-00631.1

The final published version of this manuscript will replace the preliminary version at the above DOI once it is available.

If you would like to cite this EOR in a separate work, please use the following full citation:

Feldl, N., and G. Roe, 2013: The nonlinear and nonlocal nature of climate feedbacks. *J. Climate*. doi:10.1175/JCLI-D-12-00631.1, in press.

© 2013 American Meteorological Society

ABSTRACT

4
5 The climate feedback framework partitions the radiative response to climate forcing into
6 contributions from individual atmospheric processes. The goal of this study is to understand
7 the closure of the energy budget in as much detail and precision as possible, within as
8 clean an experimental set-up as possible. For an aquaplanet simulation under perpetual
9 equinox conditions, we account for rapid tropospheric adjustments to CO₂ and diagnose
10 radiative kernels for this precise model set-up. We characterize the meridional structure
11 of feedbacks, heat transport, and nonlinearities in controlling the local climate response.
12 Our results display a combination of positive subtropical feedbacks and polar amplified
13 warming. These two factors imply a critical role for transport and nonlinear effects, with
14 the latter acting to substantially reduce global climate sensitivity. At the hemispheric scale,
15 a rich picture emerges: anomalous divergence of heat flux away from positive feedbacks
16 in the subtropics; nonlinear interactions amongst and within clear-sky feedbacks, which
17 reinforce the pattern of tropical cooling and high-latitude warming tendencies; and strong
18 ice-line feedbacks that drive further amplification of polar warming. These results have
19 implications for regional climate predictability, by providing an indication of how spatial
20 patterns in feedbacks combine to affect both the local and nonlocal climate response, and
21 how constraining uncertainty in those feedbacks may constrain the climate response.

1. Introduction

The power of the climate feedback framework lies in its ability to reveal the energy pathways by which the system adjusts to an imposed forcing, such as an increase in atmospheric CO₂ concentration. These internal adjustments may include changes in physical processes that control the distribution of clouds, water vapor, sea ice, and the vertical structure of temperature, which in turn act to amplify or dampen the surface temperature response to the forcing; these are the climate feedbacks. Further, the system may also adjust by redistributing energy between different latitudes, either by atmospheric or oceanic transport, or both. Understanding the relative importance and effectiveness of these different pathways is crucial for predicting the climate response to a perturbation.

We begin by reviewing the underpinnings of feedback analysis (e.g., Roe 2009). Climate feedbacks are closely related to the change in top-of-atmosphere (TOA) net radiative flux between two climate states, ΔR , which can be written as a Taylor series expansion in global-mean surface temperature change, $\Delta\bar{T}_s$:

$$\Delta R = A + B\Delta\bar{T}_s + \mathcal{O}\Delta\bar{T}_s^2. \quad (1)$$

The terms in Equation 1 can represent global averages, or be functions of latitude or grid cell, and in principle, one could alternatively choose to make the expansion in local temperature change (e.g. Crook et al. 2011; Armour et al. 2012). The sign convention is such that a positive radiative flux warms the system. The first term on the right-hand side, A , includes the external forcing itself, along with all changes in the energy balance that are independent of surface temperature change (i.e., semi-direct effects, see Section 2b). We refer to A as the climate forcing. The second term, $B\Delta\bar{T}_s$, reflects radiative flux changes that are linearly dependent on the system response $\Delta\bar{T}_s$; these are the classical feedback processes. Here, the sign of the feedback term is negative when the system is stable (i.e., a net negative feedback). The third component, $\mathcal{O}\Delta\bar{T}_s^2$, represents higher-order terms, which

46 may reflect nonlinearities within individual processes or nonlinear interactions amongst dif-
 47 ferent processes. In general, ΔR may be accommodated by either local heat storage or by a
 48 change in the divergence of atmospheric or oceanic heat transport ($\sim \Delta(\nabla \cdot F)$). We only
 49 present equilibrium calculations, so local heat storage can be neglected. Therefore, for the
 50 remainder of this study $\Delta(\nabla \cdot F)$ and ΔR are interchangeable. Further, in the global mean
 51 $\Delta(\nabla \cdot F) = 0$, and the feedback and nonlinear term must balance the forcing. Finally, Equa-
 52 tion 1 is commonly written in a simplified form, with the nonlinear term $\mathcal{O}\Delta\bar{T}_s^2$ assumed
 53 minor and neglected (e.g. Senior and Mitchell 2000; Gregory et al. 2004; Soden and Held
 54 2006), though we expressly evaluate it herein.

55 The goal of this study is to understand the closure of the TOA energy balance in as much
 56 detail and precision as possible. Doing so allows us to characterize the relative importance of
 57 the four terms in Equation 1—heat transport, forcing, feedbacks, and the nonlinearities—in
 58 controlling the local climate response. We carefully diagnose the climate forcing, taking into
 59 account the semi-direct (i.e., temperature independent) response of the atmosphere to CO₂
 60 changes, and we derive the linear part of the response (i.e., the feedbacks) using radiative
 61 kernels explicitly calculated for our precise model set-up. In addition, we run our experiment
 62 in an idealized aquaplanet model with perpetual equinox conditions and a mixed-layer ocean,
 63 which minimizes complexities in the results.

64 Equation 1 can be rewritten using notation more common to the climate-feedbacks lit-
 65 erature, and the nonlinear term can be expressed as a residual \mathcal{R} :

$$\underbrace{\mathcal{R}}_{\text{residual}} = \underbrace{\Delta R}_{\text{transport}} - \underbrace{\left[\left(\begin{array}{c} \lambda_x \\ x \end{array} \right) \Delta\bar{T}_s + \Delta\tilde{R}_f \right]}_{\text{combined feedback and forcing}} = \mathcal{O}\Delta\bar{T}_s^2. \quad (2)$$

66 As discussed later, due to the methodology we use for determining the cloud feedback, the
 67 residual in this study applies only to the clear-sky physics (Section 2c and Appendix A).
 68 In our results we interpret this residual as the nonlinear term. Although we have tried to
 69 be diligent in rooting out common approximations that would contribute artificially to the

70 residual, some may linger, and we return to this point in later sections.

71 Recall that ΔR in Equation 2 is the change in net TOA radiative flux and that it must be
72 equal to the change in convergence of horizontal atmospheric heat flux, $\Delta(\nabla \cdot F)$; we refer to
73 this term as “transport” for convenience. The forcing $\Delta\tilde{R}_f$ is equivalent to A in Equation 1,
74 where for clarity the tilde has been introduced to indicate the inclusion of semi-direct effects
75 (discussed in Section 2b). We replace B with $\sum_x \lambda_x$. In much of the climate literature λ_x
76 are known as feedback parameters, which we adopt here for consistency with earlier work,
77 though we note this departs from conventional definitions (e.g. Bode 1945; Schlesinger 1985;
78 Roe 2009). Physically the terms in the λ_x series simply reflect the linear decomposition of
79 changes in the TOA energy budget (x represents water vapor, surface albedo, cloud, Planck
80 and lapse rate feedbacks). Bony et al. (2006) provide a comprehensive review of the various
81 climate feedbacks relevant on interannual to multidecadal timescales, and we will elaborate
82 on the individual terms in following sections.

83 By construction, the feedback framework only provides an approximation to the actual
84 TOA radiative flux changes, and hence to climate sensitivity. As mentioned above, a goal of
85 this study is to understand the degree of approximation, and to the extent possible, assign
86 physical meaning to the structure of the nonlinear term. How important are nonlinearities for
87 the local energy balance, and do they provide insights into understanding ubiquitous features
88 of climate change, such as polar amplification? While a handful of studies have quantified
89 the linear approximation with respect to magnitude of forcing (Colman et al. 1997; Colman
90 and McAvaney 2009; Jonko et al. 2012), we are unaware of any that emphasize the spatial
91 pattern of *interactions* amongst clear-sky feedbacks. Further, how well must the forcing be
92 represented to evaluate the energy balance? This question is partly motivated by recent
93 work that has demonstrated a narrowing of the intermodel-spread in cloud feedback when
94 rapid tropospheric adjustments are counted as part of the forcing (e.g., Andrews and Forster
95 2008).

96 We are motivated by a need to understand the implications of nonlinear and nonlocal

97 feedbacks on regional climate predictability. Our first objective is a precise quantification
98 of nonlinear interactions between feedbacks, using our idealized aquaplanet simulation. We
99 also present an independent evaluation of the nonlinearity, in order to add physical meaning
100 to our characterization. Our second objective is to understand the relative importance of
101 contributions due to feedbacks, meridional heat transport, nonlinearities, and forcing to the
102 spatial pattern of warming. In particular, this allows us to assess how local processes (i.e.,
103 feedbacks) affect nonlocal responses via transport. In essence, we have extended the feedback
104 framework, conventionally applied to deconstructing global climate sensitivity, in order to
105 evaluate the role of nonlinearities and dynamical effects on local temperature change.

106 **2. Analysis**

107 *a. Aquaplanet model*

108 We employ the Geophysical Fluid Dynamics Laboratory Atmospheric Model 2 (GFDL
109 AM2) in its aquaplanet configuration. We specify perpetual equinox and daily-mean so-
110 lar zenith angle. The ocean is represented as a 20-m mixed layer. Sea ice is treated as
111 infinitesimally thin; the ocean albedo is increased to 0.5 where surface temperature drops
112 below 263 K, but no ice thermodynamics are present in the experimental set-up. The crit-
113 ical temperature for sea-ice formation was chosen to reproduce a realistic ice-line latitude,
114 when compared to the modern climate. A full description of the AM2 is provided by the
115 GFDL Global Atmospheric Model Development Team (2004). This idealized configuration
116 allows us to cleanly isolate the atmospheric response to CO₂ in the absence of coupled ocean
117 physics, land-ocean contrast, land-surface processes, seasonal and diurnal cycles, and aerosol
118 forcing. Our perturbation is achieved by an instantaneous doubling of CO₂, and then by
119 integrating the model out to equilibrium.

120 Figure 1 shows climatological surface temperature and outgoing longwave radiation (OLR)
121 for control and perturbation experiments, as well as the differences, for the last ten years

122 of our 30-year integration. For this model set-up, doubling CO₂ results in a global-mean
123 temperature increase of 4.69 K, a climate sensitivity that sits slightly above the upper end
124 of the IPCC AR4 “likely” range (Solomon et al. 2007) and of AR5 models (Andrews et al.
125 2012). The shape of the temperature response as a function of latitude is characterized
126 by strong polar amplification; warming peaks at 11.5 K in high northern latitudes, more
127 than twice the global-mean. For comparison, Hwang et al. (2011) find that Arctic warming
128 ranges from 2 to 3 times the global mean for CMIP3 simulations. Maxima in OLR occur
129 over the dry subtropics, and the global-mean OLR for the control run is 235 W m⁻², which
130 is about 10% larger than April climatology provided by NOAA-CIRES Climate Diagnostics
131 Center¹. In response to CO₂ doubling, there is a strong equatorial peak in Δ OLR associated
132 with a 16% decrease in cloud fraction in the tropical upper-troposphere (see Fig. 4b). In
133 nature, as in more complex models, the meridional structure of annual-mean OLR is blurred
134 by seasonal variations in the position of the intertropical convergence zone (ITCZ), and by
135 zonal asymmetries due to land-ocean contrast. The choice of perpetual equinox conditions,
136 which produces a permanent equatorial ITCZ, leads to a focusing of many of the climate
137 fields about the equator, which will also become apparent when we examine the patterns of
138 water vapor and cloud feedbacks. This is a trade-off: we gain a clear picture of the feedback
139 patterns and their dynamical causes in this idealized model, but must be more cautious
140 about a direct application of the results to nature.

141 *b. Determination of radiative forcing*

142 Previous feedback studies have commonly assumed a spatially uniform radiative forc-
143 ing based on estimates of the global mean (e.g. Soden et al. 2008). However the pattern
144 of radiative forcing can be strikingly nonuniform, as we will show. Since our goal in this
145 study is to close the energy balance as nearly as possible, an updated approach is desired
146 that accounts for this spatial variability and is exact to our experimental set-up. Various

¹Available online at <http://www.cdc.noaa.gov>.

147 definitions of radiative forcing are discussed in Hansen et al. (2005). We consider two meth-
148 ods: stratosphere-adjusted, in which the stratosphere is allowed to adjust radiatively to the
149 presence of the forcing agent; and fixed-SST forcing, in which the troposphere is allowed
150 to adjust as well. For a feedback analysis, the latter is to be strongly preferred since it
151 accounts for all changes in forcing that are independent of surface temperature change. In
152 other words, it is closest to the definition of A in Equation 1. We describe each forcing
153 approach in more detail below.

154 The first method, stratosphere-adjusted radiative forcing, is calculated offline from the
155 GFDL radiative transfer code, following definitions provided in the IPCC Third Assessment
156 Report (Appendix 6.1 of Ramaswamy et al. 2001; Hansen et al. 2005). Under this classical
157 “fixed dynamical heating” framework, the stratosphere is allowed to adjust to the forcing
158 prior to calculating the TOA flux change. In other words, changes in the downward flux from
159 the stratosphere, as a result of stratospheric temperature change, are assumed to be part of
160 the forcing. The resulting quantity is sometimes called the “adjusted” radiative forcing, and
161 it is relevant for CO_2 perturbation experiments because the adjustment of the stratosphere
162 is argued to be fast compared to both the tropospheric response and the lifetime of the
163 forcing agents (Hansen et al. 2005). Once the stratosphere has adjusted to its new radiative-
164 dynamical equilibrium, the change in flux at the tropopause and at the TOA are identical.
165 The solid gray line in Figure 2a shows the stratosphere-adjusted radiative forcing. It has a
166 global mean value of 3.4 W m^{-2} and, notably, varies by about a factor of two as a function of
167 latitude. The spatial pattern of the forcing is controlled by variations in surface temperature
168 and high-level cloudiness (Shine and Forster 1999). Adding CO_2 beneath a region of extensive
169 climatological cloud cover has less impact on TOA radiative fluxes. Highest values are thus
170 found in the warm, cloud-free subtropics.

171 The second method, fixed-SST forcing, focuses on $\Delta\tilde{R}_f$ as the climate forcing applied to
172 the system *independent of and prior to a surface temperature response*. This definition is
173 spurred by recent modeling results that have demonstrated semi-direct, tropospheric adjust-

174 ments in response to CO₂ (in addition to the direct radiative effect of the greenhouse gas
175 itself), which precede substantial surface warming and affect the TOA radiation balance. In
176 particular, several studies (e.g., Andrews et al. 2011) have emphasized the importance of the
177 cloud response operating over timescales less than one month. This rapid cloud adjustment
178 manifests primarily as a shortwave effect of <1 W m⁻², which Colman and McAvaney (2011)
179 suggest is driven by a decrease in relative humidity and cloud fraction in regions of enhanced
180 heating at mid-to-lower levels in the troposphere. Other hypotheses involve shoaling of the
181 planetary boundary layer due to suppressed surface heat fluxes (Watanabe et al. 2011) or
182 reductions in entrainment (Wyant et al. 2012). Since it does not constitute a response to
183 surface temperature change, any effect of rapid tropospheric adjustment is more properly
184 combined with the forcing term. Failure to take this rapid adjustment into account as a
185 forcing may bias the cloud feedback calculation.

186 We therefore perform a fixed-SST experiment, which is able to incorporate the rapid
187 tropospheric adjustment to CO₂ prior to surface temperature change—in essence, turning off
188 the feedbacks. A general critique of fixed-SST experiments in standard GCM configurations
189 is that warming still occurs over land surfaces and sea ice, undermining the goal of having no
190 surface response. However the aquaplanet integrations do not suffer from this inconsistency.
191 We can easily fix surface temperature everywhere, and in effect equate the fixed-SST forcing
192 of Hansen et al. (2005) with the “adjusted troposphere and stratosphere forcing” of Shine
193 et al. (2003). The fixed-SST experiment is integrated for 40 years with zonally-symmetric
194 and symmetric-about-the-equator specified SSTs (taken from the final year of our control
195 run). It is otherwise identical to our model set-up for the feedback analysis. The forcing is
196 then simply the change in net TOA radiative flux between 1×CO₂ and 2×CO₂ scenarios,
197 with the first year discarded.

198 The solid black line in Figure 2a shows the climate forcing $\Delta\tilde{R}_f$, including both ex-
199 ternal forcing and rapid tropospheric adjustments. It has a global-mean value² of $3.8 \pm$

²The standard error (i.e., standard deviation of the mean) of the fixed-SST forcing is calculated from the monthly change in net TOA radiative flux after the doubling of CO₂. The estimated degree of uncertainty

200 0.2 W m⁻², close to that of the uniform forcing (Myhre et al. 1998). The fixed-SST and
201 stratosphere-adjusted forcings share some similarities, particularly in the southern hemi-
202 sphere, with maxima in the subtropics. However the fixed-SST forcing is characterized by
203 notable, and perhaps surprising, hemispheric asymmetries. In fact, these asymmetries reflect
204 exactly the physics we intended to capture in the forcing estimate. The clear-sky forcings
205 (solid lines in Fig. 2b) are quite similar for both methods and hence it is the shortwave
206 response of clouds to CO₂ (hashed line), which explains the variability, consistent with the
207 proposed rapid cloud adjustment. In addition to the noisiness of the calculation, some of
208 the hemispheric asymmetry may also be due to the perpetual equinox conditions that limit
209 interaction between the hemispheres.

210 In the analysis that follows we predominantly use this fixed-SST forcing because it is
211 nearest to our definition of a temperature-independent forcing, as presumed by the feedback
212 framework, and because we believe it represents genuine variability in the forcing. The
213 relatively small impact of this hemispheric asymmetry in forcing can be gauged from our
214 results (see Fig. 3) and will be discussed in more detail in later sections; the differences also
215 serve as a rough indication of how uncertainty in forcing influences the meridional structure
216 of feedbacks.

217 *c. Kernels and feedbacks*

218 We apply the radiative kernel method of calculating climate feedbacks, following Soden
219 and Held (2006) and Soden et al. (2008). The kernel represents the TOA radiative adjustment
220 due to a differential nudge in the climate fields, and is calculated separately for changes in
221 temperature, water vapor, and surface albedo. It can be thought of as a sensitivity matrix.
222 A strength of our analysis is that we explicitly calculate radiative kernels for our precise
223 experimental set-up, thus removing one of the most commonly-cited ambiguities associated

for the 40-year integration is comparable to values cited by previous studies (e.g., 0.3 W m⁻² in Shine et al.
2003).

224 with this method (i.e., a mismatch between models used in kernel-generation and feedback-
225 calculation, as occurs in intermodel comparisons; Zelinka and Hartmann 2012).

226 Radiative kernels are not the only approach for calculating feedbacks, and a comparison
227 of various techniques can be found in Yoshimori et al. (2011). Briefly, kernels are a popular
228 choice for intermodel comparisons because the calculation is based on a small and arguably
229 non-model-specific perturbation (Soden and Held 2006), though they break down for suffi-
230 ciently different mean states, such as under CO₂ octupling (Jonko et al. 2012). Non-kernel
231 feedback calculations include partial radiative perturbation (PRP) and regression. The PRP
232 method (Wetherald and Manabe 1988; Colman 2003) suffers from computational expense.
233 The regression method of Gregory et al. (2004) is complicated by ambiguities associated
234 with transient adjustments that can result in a poorly-constrained (or even misdiagnosed;
235 Armour et al. 2012) feedback estimate, particularly when local scales are of interest, and
236 by the inability to separately evaluate temperature, water vapor, and surface changes. Fi-
237 nally, recent studies have also proposed to reformulate the kernel framework around relative
238 humidity, rather than specific humidity, thus removing the correlation between water vapor
239 and lapse rate changes (Held and Shell 2012; Ingram 2012). However this rearrangement
240 of energy flux changes into different individual feedbacks does not affect the total linear
241 feedback nor the characterization of the nonlinear term, which is the focus of the present
242 study.

243 Kernels show particular promise where nonlinear interactions are of interest. All feedback
244 methods seek to characterize the linear decomposition of TOA radiative flux changes into the
245 relative contributions from different physical processes. The PRP method is arguably the
246 most exact decomposition of the differences between two climate states because the total
247 (i.e., discrete) changes are used in the radiative calculations. However given our goal to
248 estimate the linearity of climate feedbacks, the kernel method, in its use of small differential
249 changes, is actually closer to the “tangent linear” approximation that is the formal basis for
250 the Taylor series expansion in Equation 1.

251 Hence, following Soden and Held (2006) and Soden et al. (2008), we compute all feedbacks
 252 (with the exception of clouds) as products of two factors. The first is the change in TOA
 253 flux due to a small perturbation in variable x , and the second is the change in x between
 254 the two equilibrium climate states ($1\times\text{CO}_2$ and $2\times\text{CO}_2$), divided by the global-mean surface
 255 temperature response.

$$\lambda_x = \frac{\partial R}{\partial x} \cdot \frac{dx}{dT_s} \quad (3)$$

256 where $\partial R/\partial x = K_x$ (i.e. the radiative kernel for x) and x represents temperature, specific
 257 humidity, and surface albedo. To create the kernels, instantaneous temperatures T , including
 258 the surface temperature T_s , are perturbed by 1 K; surface albedo α is perturbed by 1%; and
 259 specific humidity q is perturbed to match the change in saturation specific humidity that
 260 would occur from a 1 K warming, assuming fixed relative humidity. We perturb T , α , and q
 261 from the control climate for each latitude, longitude, time, and pressure level. The kernels are
 262 calculated from one year of instantaneous eight-times daily model output, using the offline
 263 radiation code. We make computations for clear skies (i.e., clouds instantaneously set to
 264 zero) as well as for all-sky conditions simulated by the model. The kernels we derive broadly
 265 resemble the kernels calculated from more realistic climate models (i.e., with land, seasonal
 266 cycles, etc.), as presented for instance in Soden et al. (2008). However the simplicity of our
 267 aquaplanet set-up means the spatial patterns of the kernels are sharper, and can be very
 268 clearly related to individual aspects of the atmospheric response. The kernels are presented
 269 and described in detail in Appendix B.

270 Feedbacks are calculated by convolving 10 years of equilibrated monthly anomalies with
 271 the 12-month kernels, in the case of temperature, water vapor, and albedo (Eqn. 3). The
 272 two parts comprising the temperature feedback are calculated from the surface temperature
 273 response applied throughout the troposphere (in the case of the Planck feedback), and the
 274 departure at each level from that uniform change (for the lapse rate feedback). We then
 275 integrate from the surface to the tropopause, defined as 100 mb at the equator and decreasing
 276 linearly to 300 mb at the poles.

277 Clouds are handled differently from non-cloud feedbacks, because the radiative effect of
 278 vertically-overlapping cloud fields is too nonlinear for the kernel method. Following Soden
 279 et al. (2008), the cloud feedback is calculated from the change in cloud radiative forcing
 280 (ΔCRF), with adjustments for cloud masking:

$$\lambda_c \Delta \bar{T}_s = \Delta CRF + (K_T^0 - K_T) dT + (K_q^0 - K_q) dq + (K_\alpha^0 - K_\alpha) d\alpha + (\Delta \tilde{R}_f^0 - \Delta \tilde{R}_f) \quad (4)$$

281 where K^0 terms are the clear-sky kernels, $\Delta \tilde{R}_f^0$ is the clear-sky forcing, and ΔCRF is de-
 282 fined as the difference between net downward radiative fluxes in all-sky (i.e., the observed
 283 meteorological conditions, including clouds if present) and clear-sky (i.e., assuming no cloud)
 284 conditions. A discussion of the effect of clouds on clear-sky feedbacks can be found in Soden
 285 et al. (2004). As a consequence of this calculation, our nonlinear term in Equation 2 refers
 286 to clear-sky physics only (see Appendix A). Neglecting to account for the cloud-masking
 287 adjustments (e.g. Cess et al. 1990; Gregory and Webb 2008) may lead to misdiagnosis of
 288 the cloud feedback, as pointed out by Colman (2003). Note that the final term of the right-
 289 hand side of Equation 4 ensures that temperature-independent changes in clouds due to CO₂
 290 forcing are not included in the cloud feedback.

291 In defining the control climate as the 1×CO₂ integration rather than as the 2×CO₂ fixed-
 292 SST integration, we run the risk of double-counting the temperature-independent response
 293 to CO₂, which has already been included with the forcing component $\Delta \tilde{R}_f$. In essence,
 294 any change in climate field can be linearly related to surface temperature (as the feedback
 295 framework presumes), or not—in which case dx in Equation 3 or more likely ΔCRF in
 296 Equation 4 could include an additional source of nonlinear behavior. However as we will
 297 demonstrate, the two metrics of forcing (the difference between which *is* the semi-direct
 298 effect of CO₂) produce feedbacks that are not substantially different, lending confidence that
 299 the effect of the temperature-independent component is small within our kernel-computed
 300 feedbacks. Further, we identify the dominant source of the residual nonlinearity (see Section

301 3c) as due to a different process entirely.

302 **3. Results**

303 *a. Feedbacks*

304 Global-mean feedbacks are presented in Table 1. We first focus on the top row, which are
305 the feedbacks calculated assuming the fixed-SST climate forcing. The temperature feedback
306 is strongly negative (i.e., stabilizing the climate): A warmer planet emits more radiation
307 to space (Planck feedback), and the weakened lapse rate, which is a consequence of moist
308 adiabatic stratification, leads to emission from an even warmer atmosphere than if lapse
309 rate were fixed (lapse rate feedback). The water vapor feedback is strongly positive because
310 humidity is highly sensitive to warming, and because moistening the atmosphere increases
311 infrared opacity and downwelling radiation. The surface albedo feedback is positive and, as
312 expected, controlled by sea-ice processes. The net cloud feedback seems to be partly driven
313 by changes in cloud fraction: the longwave cloud feedback is associated with the insulating
314 effect of widespread increases in high cloud fraction, and the shortwave cloud feedback is
315 associated with widespread decreases in reflective low cloud fraction (Fig. 4b). These global-
316 mean feedbacks are in broad agreement with coupled-model studies, though our shortwave
317 cloud feedback is on the high end of the range (e.g., Randall et al. 2007). Preliminary results
318 indicate the absence of a tropical Walker circulation in the aquaplanet to be a controlling
319 factor in the shortwave component of the cloud feedback, which may help to explain the
320 relatively high sensitivity exhibited by our aquaplanet.

321 The sum of the linear feedbacks, which we call “total feedback” for convenience, is small
322 and negative ($-0.49 \text{ W m}^{-2} \text{ K}^{-1}$). If the assumption of linearity were correct, then the global
323 climate sensitivity would be calculated as $\Delta \overline{T}_s = \overline{\Delta R_f} / \overline{\sum_x \lambda_x} = 7.7 \text{ K}$, rather than the
324 actual value of 4.69K. This points, then, to a substantial role for the nonlinear term. While
325 it is smaller in magnitude than any individual feedback, comparison of the last two columns

326 of Table 1 shows that the nonlinear term is 67% of the total feedback. Thus nonlinearities
327 are of comparable importance to the linear feedbacks in affecting the TOA energy balance,
328 at least in a global-mean sense and for this model set-up. Moreover this term tends to have
329 a compensating role, in that it reduces global climate sensitivity. The importance of the
330 nonlinearity in the global mean is further motivation to analyze the spatial pattern of the
331 nonlinearity and feedbacks.

332 How does the magnitude of our nonlinearity compare to previous work? Though reporting
333 conventions vary for the validity of the linear approximation, we can perform two crude
334 comparisons. First, we estimate the equivalent nonlinear term from other studies by applying
335 their cited values of feedbacks, forcing, and climate sensitivity to our Equation 2. Thus our
336 nonlinear term, $-0.33 \text{ W m}^{-2} \text{ K}^{-1}$, is comparable in magnitude to estimates 0.39 W m^{-2}
337 K^{-1} (Soden and Held 2006; Soden and Vecchi 2011, for GFDL CM2.1) and 0.13 W m^{-2}
338 K^{-1} (Shell et al. 2008, for CAM3), though our sign is different. Second, as an alternative
339 approach, we instead assume the nonlinear term can be expressed in the form $c\Delta\bar{T}_s^2$, such
340 that the value of the coefficient c is a measure of the degree of nonlinearity. Roe and Armour
341 (2011, their supplementary materials) report $|c| \leq 0.06 \text{ W m}^{-2} \text{ K}^{-2}$ from a dozen different
342 studies, with no consensus on sign. For our present study, the nonlinear term divided by
343 $\Delta\bar{T}_s$ ($-0.33 \text{ W m}^{-2} \text{ K}^{-1}$ per 4.69 K) gives $c = -0.07 \text{ W m}^{-2} \text{ K}^{-2}$. Thus the magnitude of our
344 nonlinear term is roughly comparable to previous research, though on the high end. This
345 may reflect our high climate sensitivity, or be a reflection of the idealized framework. That
346 the nonlinear term is such a large percentage of the total linear feedback is a consequence of
347 the total feedback being small.

348 For the sake of comparison, Table 1 also shows global-mean feedbacks for the stratosphere-
349 adjusted radiative forcing. Due to the way in which the feedbacks are calculated, the choice
350 of forcing can only affect the cloud feedback (compare Eqns. 3 and 4), total feedback, and
351 residual. Overall, the differences in these terms as a function of forcing are fairly small.
352 In fact, we find that the rapid tropospheric adjustment (included in the fixed-SST forcing)

353 accounts for only a 16% decrease in the global shortwave cloud feedback, which is less
354 than cited in previous studies (Colman and McAvaney 2011; Andrews et al. 2011). The
355 discrepancy may reflect the inability of non-aquaplanet models to easily constrain land-
356 temperature change, or alternately, a genuine difference in cloud response between models
357 or model configurations. Hereafter we use only the fixed-SST forcing.

358 We now turn to the meridional structures of the feedbacks, which are shown in Figure
359 3. The first thing to note is that, converted to the same scale, the climate forcing has a
360 value of about 0.5-1.2 W m⁻² K⁻¹ (2.5 to 5.5 W m⁻² per 4.69 K). In other words, Figure
361 3 shows that the local adjustments by atmospheric process (i.e., feedbacks) are in general
362 larger than the forcing itself. Another striking feature is that the Planck feedback is most
363 strongly stabilizing (i.e., most negative) at high latitudes. This is in contrast to the simple
364 picture one might naively expect from the Stephen-Boltzmann Law, wherein the change in
365 outgoing flux varies as $4\sigma T^3$ and therefore is greatest in the tropics. However from Equation
366 3 we see that the Planck feedback is the product of the temperature kernel, $\partial R/\partial T$, whose
367 amplitude indeed peaks at low latitudes (Fig. B1a in Appendix B), and the ratio $dT_s/d\bar{T}_s$.
368 Given strong polar amplification (i.e., $dT_s \gg d\bar{T}_s$), this is enough to produce a Planck
369 feedback that maximizes in magnitude at high latitudes. If feedbacks were instead defined
370 as a Taylor series expansion around the local surface temperature change, as in Section 3b,
371 then the pattern would be quite different (Feldl and Roe 2013). The lapse rate feedback
372 is most negative where temperatures follow a moist adiabat (i.e., in the tropics) and most
373 positive in the presence of high-latitude temperature inversions. The combined temperature
374 feedback (Planck plus lapse rate, not shown) is strongly negative and peaks in magnitude
375 at the equator.

376 The water vapor feedback is positive at all latitudes. However, the water vapor feedback
377 is strongest where humidity is most sensitive to warming (c.f. Fig. B1b in Appendix B).
378 These conditions occur in the subtropics and tropics, albeit the water vapor feedback is
379 weaker along the equator due to high cloud masking of the tropical moistening at the ITCZ.

380 A key point here is that the water vapor feedback is not independent of the cloud fields,
381 and this interaction between feedbacks hints at the presence of nonlinearity. In other words,
382 water vapor changes under clouds have a reduced effect on the TOA fluxes, compared to
383 cloud-free conditions. The water vapor feedback pattern is particularly sharp due to our
384 perpetual equinox conditions (i.e., lack of seasonality) and aquaplanet configuration. In
385 other words, we anticipate that the annual average over seasons would be smoother (i.e.,
386 exhibiting a less pronounced tropical minima) than the annual average over twelve months
387 of a stationary ITCZ.

388 The net cloud feedback is positive everywhere except at high latitudes. The breakdown
389 into shortwave and longwave components is shown in Figure 4. Changes in cloud fraction
390 (Fig. 4b) are consistent with much of the meridional structure, though changes in cloud
391 altitude and optical depth may also play a role (e.g., Colman et al. 2001; Zelinka et al.
392 2012). Recall that warming associated with a positive cloud feedback can occur by *decreases*
393 in bright clouds (i.e., the SW effect) or *increases* in high, insulating clouds (i.e., the LW
394 effect). The first thing to note from Figure 4a is that the shortwave component dominates
395 the sign of the net response observed in Figure 3. Hence the peak in the net cloud feedback
396 in the tropics is consistent with a decrease in cloud fraction at all levels, but especially in
397 the upper troposphere (with some compensation between a positive shortwave and negative
398 longwave cloud feedback); these cloud fraction changes are consistent with a weakening of the
399 Hadley Cell. The negative net cloud feedback in the high latitudes coincides with an increase
400 in low, bright clouds, and a poleward shift of the storm track. The positive net cloud feedback
401 at intermediate, extratropical latitudes is consistent with widespread decreases in low cloud
402 fraction (i.e., positive shortwave cloud feedback) and increases in high cloud fraction (i.e.,
403 positive longwave cloud feedback).

404 The surface albedo feedback is locally the strongest positive feedback, though it is con-
405 fined to the vicinity of the ice line (Fig. 3). Consistent with expectations, reduction of
406 sea-ice cover and the corresponding decrease in surface albedo in a warmer world lead to

407 an increase in absorbed solar radiation, and further warming. Note that a compensation
408 between positive albedo and negative shortwave cloud feedback is observed in Figures 3 and
409 4. This is a robust result across intermodel comparisons (Zelinka and Hartmann 2012; Crook
410 et al. 2011), though the extent to which clouds are modified by increases in water vapor and
411 evaporation over newly-open water is not easily constrained in a linear feedback framework
412 (Bony et al. 2006; Stephens 2005). Previous studies have also pointed to an increase in
413 high-latitude cloud optical depth due to increases in cloud water content, as well as phase
414 changes (Senior and Mitchell 1993; Tsushima et al. 2006; Zelinka et al. 2012).

415 The meridional structure of the total feedback is the sum of the individual feedbacks, and
416 is shown in Figure 3. Overall, the feedback is negative and stabilizing at high-latitudes (with
417 the exception of the ice-line, where the albedo feedback is strong enough to result in a total
418 feedback approaching zero). This locally negative total feedback might lead one to expect a
419 weak surface temperature response. Yet Figure 1 shows strong polar amplification. Further,
420 the total feedback is generally positive in the subtropics, which would imply a locally unstable
421 climate—and an infinite response. Clearly then, either substantial redistribution of energy
422 by meridional transport must occur, or else nonlinear interactions must arise. This finding
423 is reminiscent of the work of Pierrehumbert (1995), in which circulation acts to shunt energy
424 from unstable to stable latitudes, which are likened to “radiator fins.” The general tendency
425 of the total feedback to become more negative towards higher latitudes can also be seen
426 in previous studies: although a large spread exists among models, Zelinka and Hartmann
427 (2012) find that the zonal-mean total feedback parameter averaged over 12 CMIP3 models
428 exhibits a tropical peak. It is not clear if their tropical peak (rather than our subtropical
429 peak) is an artifact of the ensemble average, or if the absence of seasonality in our idealized
430 framework accounts for the difference in location of the unstable domain. In any case, the
431 combination of strong polar amplification and positive subtropical feedbacks implies critical
432 roles for meridional transport and/or nonlinearities, to which we now turn.

433 The trade-off between meridional transport and the local demands of linear feedbacks

434 is reflected in the three-term energy balance of Equation 2. The solid gray line in Fig-
 435 ure 5 shows the meridional structure of the combined feedback and forcing term (i.e.,
 436 $(\sum_x \lambda_x) \Delta \bar{T}_s + \Delta \tilde{R}_f$). The positive values equatorward of approximately 40° represent a
 437 local warming tendency. In a perfectly linear world, the changes in transport (dashed line)
 438 would exactly balance the combined feedbacks and forcing. However in a nonlinear world,
 439 that adjustment is incomplete, and the remainder of the energy balance is accommodated by
 440 the nonlinear, or residual, term (solid black line in Fig. 5). In particular, there is increased
 441 meridional transport out of the subtropics, and the shape of this term closely mirrors that of
 442 the feedback-plus-forcing. In other words, in the subtropics, the system attempts to diverge
 443 heat away from the region of strong positive feedback, but transport alone does not fully
 444 accommodate this energy. The balance is taken up by the nonlinear term, which provides
 445 a cooling tendency in the low latitudes (equatorward of 50°) and a warming tendency else-
 446 where. Hence in addition to compensating the global sensitivity, the nonlinear term plays
 447 an important, compensating role at many latitudes: It opposes the positive feedback in the
 448 tropics, and likewise offsets the negative feedback at high latitudes. Further, the nonlinear
 449 term is minimized (i.e., the assumption of linearity works best) in the midlatitudes; a nega-
 450 tive total feedback is balanced by anomalous heat convergence at 45° . Our ability to assess
 451 the nonlinear contribution is a key strength of our approach.

452 *b. Polar amplification*

453 Polar amplification is a striking feature of all climate models predictions and is also
 454 observed in global temperature trends (Solomon et al. 2007). In our simulation we see two
 455 scales to the polar amplification: an enhancement of the temperature response polewards of
 456 about 30° , and a much larger enhancement polewards of 60° . Polewards of 60° , the average
 457 warming is 2.2 times the global-mean response; this degree of amplification is consistent
 458 with other studies (Hwang et al. 2011; Holland and Bitz 2003). We can apply the feedback
 459 framework toward understanding polar amplification in terms of the spatial patterns of

460 climate feedbacks, forcing, heat transport, and nonlinearities. In what follows, we pursue
 461 the apparently contradictory result that the temperature response is largest in regions where
 462 the feedback is most stabilizing (compare Figs. 1 and 3).

463 Equation 2 can be rewritten with local temperature change ΔT_s substituted for global-
 464 mean $\Delta \bar{T}_s$, and the Planck feedback λ_P separated from the non-Planck feedbacks $\sum \lambda_{NP}$:

$$\Delta T_s = \frac{1}{\lambda_P} \left[\Delta R - \left(\begin{matrix} & & \\ & & \lambda_{NP_i} \\ & & \end{matrix} \right) \Delta T_s - \Delta \tilde{R}_f - \mathcal{R} \right]. \quad (5)$$

465 In essence, we normalize the terms in the energy balance by the Planck feedback. This
 466 weighting avoids an undefined surface temperature response where the total feedback goes
 467 to zero. The feedback term in Equation 5 is also more similar in form to the conventional
 468 definition where feedback factor $f = -\lambda_{NP}/\lambda_P$ (e.g., Roe 2009). Thus the pattern of local
 469 temperature response is given as the partial temperature change attributed to each term on
 470 the right-hand side of Equation 5; this decomposition is also utilized by Crook et al. (2011).
 471 These individual contributions as a function of latitude are presented in Figure 6, together
 472 with the total surface temperature change, shown in grey. As a reminder, the non-Planck
 473 feedbacks include lapse rate, water vapor, surface albedo, and cloud feedbacks.

474 The forcing produces a small and uniform warming of 0.9-1.6 K (red line, Fig. 6).
 475 This contribution to surface temperature change is not substantially different when the
 476 stratosphere-adjusted forcing is instead used (not shown). In other words, the previously
 477 noted asymmetries in forcing are small compared to the other terms in affecting surface
 478 temperature. The nonlinear term is also small (green line, ± 1.6 K) and, as expected from
 479 Figure 5, cools the tropics and warms the high latitudes, contributing to the polar-amplified
 480 shape of the warming pattern. On average the transport term also exhibits a pattern of
 481 tropical cooling and high-latitude warming, consistent with a poleward export of heat from
 482 the tropics, though its meridional structure and magnitude are more variable. The non-
 483 Planck feedbacks provide a warming tendency at all latitudes, and are the major contributor

484 to the more than 10 K warming near the ice-line. In general, non-Planck feedbacks and
485 transport exhibit strong compensation, while the nonlinear term and forcing make smaller
486 contributions to surface temperature change and with less meridional variability. Overall
487 then, the enhancement of the *average* response poleward of 30°, relative to the response
488 equatorward of 30°, may be attributed predominantly to the change in sign of the transport
489 term (and to a lesser degree, the nonlinear term). The pole-to-equator *shape* of the polar
490 amplification is largely explained by the combined effects of feedbacks and transport.

491 The further amplification of surface temperature polewards of 60° may be characterized
492 in two parts: non-Planck feedbacks (particularly surface albedo, longwave cloud, and lapse
493 rate feedbacks, see Figs. 3 and 4) from 60-70°, and meridional heat transport of 4.7 K
494 poleward of 70°. The strong warming tendency of the non-Planck feedbacks at the ice-
495 line is partially offset by the transport term (i.e., a cooling tendency due to heat export).
496 Polewards of the ice-line there is anomalous convergence of at least a portion of this exported
497 heat, which maintains the enhanced warming right to the poles. At the poles, none of the
498 terms act as cooling tendencies. Hence we find a consistent picture at both hemispheric and
499 regional scales, in which local temperature change is controlled by anomalous heat divergence
500 away from regions of strong positive feedbacks (i.e., the ice-line and the subtropics) and
501 convergence into regions of more negative feedbacks (i.e., the midlatitudes and poles).

502 The influence of the Planck weighting in Equation 5 is demonstrated in the lower panel
503 of Figure 6. The dashed line shows how the predicted surface warming would change if the
504 global-mean weighting $\overline{\lambda_P^{-1}}$ had been used in Equation 5, instead of the full spatial field. The
505 meridional structure of the Planck feedback, which increases in magnitude toward the poles
506 (see Fig. 3), contributes an additional 23% warming in the high latitudes (poleward of 60°)
507 and 15% cooling in the subtropics (5-25°). Thus the Planck feedback comes in at tertiary
508 importance, behind the other feedbacks and transport, in explaining polar amplification,
509 though its approximately 2 K high-latitude warming is distributed amongst the other terms
510 and cannot be easily isolated.

511 Our results have demonstrated the importance of meridional heat fluxes to the system
512 response. We next consider the breakdown of the transport term into changes in latent and
513 dry-static energy flux, following Trenberth and Stepaniak (2003) and Hwang and Frierson
514 (2010). As part of the calculation, we subtract the surface flux from the TOA flux, in order
515 to solve for the total atmospheric (i.e. moist-static energy) budget; the surface flux includes
516 contributions from net downward radiation at the surface, sensible heat flux, and latent heat
517 flux due to evaporation and melting snowfall into the ocean. We find the change in surface
518 flux to be smaller than $\pm 0.73 \text{ W m}^{-2}$ at all latitudes and negligible in the global mean.
519 The northward latent energy flux is calculated as the integral, with respect to latitude, of
520 evaporation minus precipitation (multiplied by the latent heat of vaporization for consistent
521 units), and the dry-static energy flux is then the residual of the latent and total atmospheric
522 fluxes.

523 Changes in northward energy fluxes are shown in Figure 7. Positive slopes in the figure
524 correspond to regions of anomalous flux divergence, and negative slopes to anomalous con-
525 vergence. The total flux change (gray line) confirms an increase in divergence away from the
526 subtropics, and an anomalous divergence away from the ice line (i.e., decreased convergence
527 with respect to the control climate). Relative to the total flux change, the latent and dry-
528 static energy components are large and mostly compensating. In the warmer climate, there
529 is an increase in latent energy flux poleward of approximately $25\text{-}30^\circ$ (solid black line). This
530 is significantly offset by a decrease in dry-static energy flux (dashed line), presumably due
531 to weaker midlatitude temperature gradients. However the total flux change is still positive,
532 and thus it is the *larger* increase in latent energy flux that explains the contribution of trans-
533 port to polar amplification polewards of 30° . Interestingly, the dry-static energy gradient
534 weakens considerably polewards of the ice line. Therefore the contribution of heat transport
535 to polar amplification at the highest latitudes (see also Hwang et al. 2011; Langen et al.
536 2012) is driven solely by the latent energy flux convergence, with no compensation from
537 dry-static energy. Figure 7 also shows an increase in equatorward latent heat flux and an

538 increase in poleward dry-static energy flux, which have the same sign as the climatological
539 fluxes.

540 *c. Source of the nonlinearity*

541 Up to this point, we have characterized the residual nonlinearity, without addressing
542 which interactions between feedbacks are responsible for the term. The core of the issue
543 is that the kernel framework assumes each variable and each vertical level are independent
544 and can be linearly combined. Whereas in fact, vertical masking of clear-sky variables, and
545 interactions amongst these variables, could complicate this picture. Analogously, it is well
546 known that clouds mask underlying tropospheric changes (Soden et al. 2004). Water vapor
547 exhibits similar behavior. Figure 8a shows changes in specific humidity between the $1\times\text{CO}_2$
548 and $2\times\text{CO}_2$ experiments. These changes show an overall moistening and are consistent with
549 a weakening and expansion of the Hadley Cell (e.g., Held and Soden 2006). The linear
550 model (e.g. kernel approach) assumes that changes in mid- and lower-tropospheric water
551 vapor have as large of an effect on the TOA as changes aloft. In actuality, the sensitivity
552 of TOA radiation fluxes to upper tropospheric humidity is well known (Cess 1975; Spencer
553 and Braswell 1997), and we expect the TOA balance to be most affected by changes aloft.
554 As a result, we anticipate that the water vapor kernel would result in an overestimate of the
555 TOA fluxes in regions of strong upper-level moistening, which would manifest as a negative
556 nonlinearity.

557 We test this hypothesis by running the actual changes at all levels ($2\times\text{CO}_2$ minus $1\times\text{CO}_2$)
558 in humidity, temperature, and surface albedo *simultaneously* through the offline radiation
559 code to calculate the magnitude of the TOA fluxes. The net radiative flux at the TOA is
560 then compared to the linear sum of the individual variables at each level, which is what the
561 kernel framework presumes. Results are shown in Figure 8b. The solid line can be thought of
562 as the difference between the GCM response and the linear approximation, or in other words,
563 it represents an independent measure of the nonlinearity. We see that this difference does

564 a rather remarkable job of capturing the magnitude and qualitative shape of the residual
565 nonlinearity (dashed line), with some obvious departures.

566 Remaining sources of nonlinearity (i.e., the difference between the two lines on Figure
567 8), can be considered with the help of Equation A2. We have already accounted for non-
568 linearities within the third term on the right-hand-side, $\sum_n \lambda_n^0 \Delta \bar{T}_s$, i.e., vertical masking
569 of, and interactions between, clear-sky feedbacks. As mentioned in Section 2b, there is also
570 the possibility of double-counting the rapid tropospheric adjustment to CO₂. However we
571 expect this contribution to be minor because the residual is nearly identical when calculated
572 with a stratosphere-adjusted, rather than fixed-SST, radiative forcing (not shown), which
573 does not suffer from double counting. Hence any remaining nonlinearities may be attributed
574 to second-order terms associated with the effect of clouds on non-cloud fields. First-order
575 terms were accounted for in Equation 4, following advances by Soden et al. (2008), and it
576 is straightforward to show that a quadratic form of Equation 4 would propagate additional
577 terms to Equation A2.

578 4. Summary and Discussion

579 In this study we have sought to understand the spatial structure of climate feedbacks and
580 the relative importance of nonlinearities and meridional heat transport. We have designed
581 a clean experiment, which seeks to remove as many of the common energy-balance approxi-
582 mations as possible. In particular, we employ a simplified aquaplanet model, and explicitly
583 calculate both fixed-SST climate forcing and radiative kernels for this precise set-up. Our
584 high climate sensitivity of 4.69 K is consistent with large subtropical regions of positive water
585 vapor and cloud feedbacks. Two regions of positive feedbacks, the subtropics and the ice-
586 line, force anomalous divergence of heat flux, which translates into polar amplification of the
587 surface temperature response via meridional latent heat transport. Nonlinearities reinforce
588 this pattern of tropical cooling and high-latitude warming tendencies, and also reduce global

589 climate sensitivity from very high to merely high. The nonlinear term can be thought of
590 as reinforcing the transport-induced warming, or, alternatively, as offsetting the total linear
591 feedback. The resulting polar-amplified warming bears the signature of feedbacks, transport,
592 and nonlinearities, but importantly, is not limited to the latitude where a particular physical
593 process is active.

594 One of the goals of this research has been to understand how local processes affect non-
595 local climate responses. The feedback pattern is characterized by strongly positive subtrop-
596 ical feedbacks, and the temperature response pattern characterized by polar amplification.
597 Clearly, meridional heat transport matters for redistributing energy. Indeed we find that
598 transport plays a role on a couple of spatial scales—from the subtropics to the mid-latitudes,
599 and from the high-latitudes, poleward. The stable midlatitudes also display interesting com-
600 plexity: abutting regions of positive feedbacks contribute to a maximum increase in heat
601 convergence at 45° , near the latitude where the nonlinearity is minimized.

602 We have further studied the source of our “nonlinear” term, which strictly represents
603 the clear-sky residual between the energy-flux changes predicted by linear theory and the
604 actual, model-produced flux changes. Though a modest contributor of at most 2K to local
605 temperature response (when normalized by the Planck feedback), the meridional structure
606 of the nonlinearity and its tendency to compensate climate feedbacks suggest a physical
607 mechanism at work. Indeed from a Taylor-series perspective, these nonlinearities can be
608 thought of as higher-order terms that do not scale linearly with surface temperature change
609 (e.g., Stephen-Boltzmann Law, or Clausius-Clapeyron relationship) or interactions between
610 feedbacks (i.e., cross-terms in the energy budget). The effect is such that, at low latitudes,
611 the feedback is less than the sum of its parts and at high latitudes it is more than the sum
612 of its parts. Generally speaking, our results caution against the use of methods in which the
613 residual is subsumed into one of the linear feedbacks (e.g., the cloud feedback of Soden and
614 Held 2006).

615 Through offline radiation experiments, we have attributed the bulk of the nonlinear

616 term to interactions within (i.e., vertical masking) and amongst clear-sky feedbacks, and
617 pointed to quadratic effects of clouds on non-cloud variables as the leading candidate for
618 remaining nonlinearity. Hence nonlinear feedbacks may represent dynamical constraints
619 within the system: changes in atmospheric circulation modulate the degree of compensation
620 between terms in the energy balance, in a way not accounted for by the linear, Taylor-
621 series approximation. For example, dynamically controlled changes in specific humidity
622 were suggested to be a major cause of the nonlinearity. Nonlinear interactions amongst
623 temperature, humidity, and surface albedo, with the latter constrained to high latitudes, are
624 active as well. It should be noted that the wholesale substitution of climate variables, all
625 levels at once, is a feature of both our offline radiation experiments and the PRP method
626 of calculating feedbacks. Thus we would expect that nonlinearities arising from the PRP
627 method to be restricted to interactions amongst (but not within, as in vertical masking)
628 feedbacks.

629 The idealized aquaplanet framework provides a unique lens on radiative interactions in a
630 changing climate, though some of our results may be a consequence of experimental design.
631 We are confident the residual does represent an approximation of the nonlinearity, because
632 (1) we made every effort to close the energy balance as nearly as possible, by diagnosing
633 radiative kernels and forcing for this model setup, and (2) two independent estimates of the
634 nonlinear term (residual and offline calculations) are consistent. However the aquaplanet
635 simulation is, by its very nature, simplified. For instance, lack of land-sea contrast will
636 have a profound effect on cloud climatologies, which we have mentioned with respect to our
637 shortwave cloud feedback—though this perhaps matters less to the nonlinearity, which is, of
638 course, a clear-sky effect. While it is reassuring that our global-mean feedbacks are within
639 the spread of intermodel comparisons (Bony et al. 2006; Randall et al. 2007), future work
640 will systematically relax the simplifying assumptions towards greater realism.

641 Possible avenues of progress include the following: (1) a comparison of the kernels from
642 $1\times\text{CO}_2$ and $2\times\text{CO}_2$ climatologies, in order to address the mean-state dependence, or exten-

643 sion of the method to calculate second-order terms; (2) the inclusion of greater realism such
644 as a seasonal cycle or ocean heat transport, which would directly affect the energy balance
645 via the transport term and indirectly through the coupling between feedbacks and surface
646 response; and (3) use of a wider range of forcings to address how feedbacks behave for larger
647 surface-temperature changes (e.g., Colman and McAvaney 2009). Furthermore, the equili-
648 brated climate change must satisfy both radiative and dynamical constraints. Sharply honed
649 numerical experiments that address the conditions under which either dynamics or radiation
650 dominates the response would be useful.

651 Our breakdown of the meridional structure of temperature response into individual com-
652 ponents (Equation 5) also illustrates some issues for the predictability of regional climate
653 change. Local feedbacks alone do not set the pattern of temperature response: atmosphere
654 (and ocean) dynamics act to redistribute energy in the system, and so one must constrain
655 the feedbacks everywhere in order to constrain the response anywhere. Figure 6 shows the
656 partial temperature change for feedbacks, transport, forcing, and nonlinearities as a function
657 of latitude in our simulations. It also provides some sense for how the meridional structure
658 of predicted climate change might vary, if improved understanding resulted in a different
659 pattern of total feedback.

660 Conventional climate feedback analysis characterizes only the energy balance and is inher-
661 ently linear by construction. We have extended that perspective in an idealized framework
662 to include nonlinear terms and to consider nonlocal effects. These must operate in the
663 real climate system and are an important component of understanding predictability. The
664 meridional structures of individual feedbacks are governed by the classical climatic zones
665 (i.e., the ITCZ, the subtropics, the midlatitudes, the poles), and thus are a consequence of
666 mean-state dynamics. However dynamical changes in the circulation pattern may modulate
667 nonlinearities and, as a consequence, global climate sensitivity. Further, the system tends to
668 allocate energy towards latitudes that can most effectively radiate to space. This means that
669 warming is minimized in the subtropics in spite of strong positive feedbacks. A complete

670 picture of climate sensitivity must unify dynamical and radiative frameworks, and it is our
671 hope that the current study offers some insights into what that may entail.

672 *Acknowledgments.*

673 The authors thank Dargan Frierson, Mark Zelinka, Ben Sanderson, Dennis Hartmann,
674 and Kyle Armour for valuable discussions; Marc Michelsen for technical assistance; and two
675 anonymous reviewers and the editor. This work was partially supported by the National
676 Science Foundation (EAR-0908558).

APPENDIX A

677

678

679

Why a clear-sky residual?

680 The clear-sky (rather than all-sky) residual is a consequence of our cloud feedback cal-
 681 culation. Equation 2 can be rearranged to give

$$\Delta R = \Delta \tilde{R}_f + \left(\begin{array}{c} \lambda_n \\ n \end{array} \right) \Delta \bar{T}_s + \lambda_c \Delta \bar{T}_s, \quad (\text{A1})$$

682 where the cloud feedback λ_c is split from the other, non-cloud feedbacks ($n = T, q, \alpha$).

683 Substituting Equation 4 into Eq. A1 gives

$$\Delta R = \Delta \tilde{R}_f^0 + \Delta CRF + \left(\begin{array}{c} \lambda_n^0 \\ n \end{array} \right) \Delta \bar{T}_s, \quad (\text{A2})$$

684 where superscripted terms represent clear-sky fluxes. Hence the residual becomes

$$\mathcal{R} = (\Delta R - \Delta CRF) - \left[\Delta \tilde{R}_f^0 + \left(\begin{array}{c} \lambda_n^0 \\ n \end{array} \right) \Delta \bar{T}_s \right], \quad (\text{A3})$$

685 or the difference between actual, model-produced clear-sky fluxes ($\Delta R - \Delta CRF$) and kernel-
 686 approximated clear-sky fluxes (the remaining terms).

APPENDIX B

687

688

Radiative kernels

689

690 To facilitate comparison with previous studies (Soden and Held 2006; Soden et al. 2008;
691 Shell et al. 2008), we present height-latitude cross sections of our perpetual equinox, aqua-
692 planet kernels. The kernels in Figure B1 represent the contribution of each level and latitude
693 to the change in longwave TOA fluxes. The temperature kernel (Fig. B1a) is strongly nega-
694 tive (i.e., stabilizing the climate) because an increase in temperature increases OLR, following
695 the Stefan-Boltzman Law. Under clear skies (not shown) the sensitivity peaks in the trop-
696 ics where temperatures are highest. However all-sky TOA fluxes are sensitive to cloud-top
697 temperature, with the largest contributions from regions of high convective clouds and sub-
698 tropical and midlatitude boundary layer clouds. The surface component of the temperature
699 kernel (Fig. B1d) exhibits cloud masking, with decreased sensitivity aligned beneath regions
700 of high cloudiness. Cloud-masking effects are also apparent in the surface albedo kernel
701 (Figure B1c), though this kernel obviously only matters near the climatological ice-line.

702 The water vapor kernel (Fig. B1b) shows the TOA radiative flux response to atmospheric
703 moistening. In calculating the kernel, specific humidity q was perturbed to match the change
704 in saturation specific humidity that would occur from a 1 K warming, assuming fixed relative
705 humidity (Soden and Held 2006). Positive values indicate that an increase in atmospheric
706 water vapor leads to an increase in infrared opacity and downwelling radiation (decreasing
707 OLR), consistent with the role of water vapor as a greenhouse gas. High sensitivity in the
708 tropics is also influenced by self-broadening of water vapor absorption spectra (Shine and
709 Sinha 1991). At high latitudes and low levels, the water vapor kernel is negative (an anti-
710 greenhouse effect); the effect of humidifying the atmosphere is to raise the emission level
711 (Cess 1975; Held and Soden 2000), leading to an increase in OLR in regions of temperature

712 inversions. The water vapor kernel peaks strongly in the climatologically dry upper tropo-
713 sphere because of the high sensitivity of saturation vapor pressure at very cold temperatures
714 and low pressures (via the Clausius-Clapeyron relationship); for fixed relative humidity at
715 200 K, specific humidity changes by 15%/K (Held and Soden 2000). Hence the pattern of
716 this kernel is tied to the assumption of fixed relative humidity. If relative humidity were
717 instead allowed to decrease, then warming would not require moistening, and it would be
718 possible to imagine a weakened water vapor response in the subtropics—though the lapse
719 rate would adjust accordingly to compensate this effect (Bony et al. 2006).

REFERENCES

- 722 Andrews, T. and P. M. Forster, 2008: CO₂ forcing induces semi-direct effects with
723 consequences for climate feedback interpretations. *Geophys. Res. Lett.*, **35** (4), doi:
724 10.1029/2007GL032273.
- 725 Andrews, T., J. M. Gregory, P. M. Forster, and M. J. Webb, 2011: Cloud adjustment and
726 its role in CO₂ radiative forcing and climate sensitivity: A review. *Surveys in Geophysics*,
727 doi:10.1007/s10712-011-9152-0.
- 728 Andrews, T., J. M. Gregory, M. J. Webb, and K. E. Taylor, 2012: Forcing, feedbacks
729 and climate sensitivity in cmip5 coupled atmosphere-ocean climate models. *Geophysical*
730 *Research Letters*, **39** (9), doi:10.1029/2012GL051607.
- 731 Armour, K. C., C. M. Bitz, and G. H. Roe, 2012: Time-varying climate sensitivity from
732 regional feedbacks, submitted to *Journal of Climate*.
- 733 Bode, H. W., 1945: *Network Analysis and Feedback Amplifier Design*. Bell Telephone Labs
734 Series, Van Nostrand Reinhold, New York, 551 pp.
- 735 Bony, S., et al., 2006: How well do we understand and evaluate climate change feedback
736 processes? *Journal of Climate*, **19** (15), 3445–3482, doi:10.1175/JCLI3819.1.
- 737 Cess, R. D., et al., 1990: Intercomparison and interpretation of climate feedback processes
738 in 19 atmospheric general circulation models. *Journal of Geophysical Research*, **95** (D10),
739 16,601–16,615.
- 740 Cess, R. D., 1975: Global climate change: an investigation of atmospheric feedback mecha-
741 nisms. *Tellus*, **27** (3), 193–198, doi:10.1111/j.2153-3490.1975.tb01672.x.

- 742 Colman, R. A. and B. McAvaney, 2011: On tropospheric adjustment to forcing and climate
743 feedbacks. *Climate Dynamics*, **36** (9), 1649–1658.
- 744 Colman, R. A., S. B. Power, and B. J. McAvaney, 1997: Non-linear climate feedback
745 analysis in an atmospheric general circulation model. *Climate Dynamics*, **13**, 717–731,
746 10.1007/s003820050193.
- 747 Colman, R. A., 2003: A comparison of climate feedbacks in general circulation models.
748 *Climate Dynamics*, **20**, 865–873, doi:10.1007/s00382-003-0310-z.
- 749 Colman, R., J. Fraser, and L. Rotstayn, 2001: Climate feedbacks in a general circu-
750 lation model incorporating prognostic clouds. *Climate Dynamics*, **18**, 103–122, doi:
751 10.1007/s003820100162.
- 752 Colman, R. and B. McAvaney, 2009: Climate feedbacks under a very broad range of forcing.
753 *Geophysical Research Letters*, **36** (1), doi:10.1029/2008GL036268.
- 754 Crook, J. A., P. M. Forster, and N. Stuber, 2011: Spatial patterns of modeled climate
755 feedback and contributions to temperature response and polar amplification. *Journal of*
756 *Climate*, **24** (14), 3575–3592, doi:10.1175/2011JCLI3863.1.
- 757 Feldl, N. and G. H. Roe, 2013: Five perspectives on feedbacks, in preparation.
- 758 GFDL Global Atmospheric Model Development Team, 2004: The new GFDL Global Atmo-
759 sphere and Land Model AM2–LM2: Evaluation with prescribed SST simulations. *Journal*
760 *of Climate*, **17** (24), 4641–4673, doi:10.1175/JCLI-3223.1.
- 761 Gregory, J. M., et al., 2004: A new method for diagnosing radiative forcing and climate
762 sensitivity. *Geophysical Research Letters*, **31** (3), doi:10.1029/2003GL018747.
- 763 Gregory, J. and M. Webb, 2008: Tropospheric adjustment induces a cloud component in
764 CO₂ forcing. *Journal of Climate*, **21** (1), 58–71, doi:10.1175/2007JCLI1834.1.

765 Hansen, J., et al., 2005: Efficacy of climate forcings. *Journal of Geophysical Research*,
766 **110 (D18)**.

767 Held, I. M. and K. M. Shell, 2012: Using relative humidity as a state variable in climate
768 feedback analysis. *Journal of Climate*, **25 (8)**, 2578–2582, doi:10.1175/JCLI-D-11-00721.1.

769 Held, I. M. and B. J. Soden, 2000: Water vapor feedback and global warming. *Ann. Rev.*
770 *Energy Environ.*, **25**, 441–475.

771 Held, I. M. and B. J. Soden, 2006: Robust responses of the hydrological cycle to global
772 warming. *Journal of Climate*, **19 (21)**, 5686–5699, doi:10.1175/JCLI3990.1.

773 Holland, M. and C. Bitz, 2003: Polar amplification of climate change in coupled models.
774 *Climate Dynamics*, **21**, 221–232.

775 Hwang, Y.-T., D. M. W. Frierson, and J. E. Kay, 2011: Coupling between arctic feedbacks
776 and changes in poleward energy transport. *Geophysical Research Letters*, **38 (17)**, doi:
777 10.1029/2011GL048546.

778 Hwang, Y.-T. and D. M. W. Frierson, 2010: Increasing atmospheric poleward energy trans-
779 port with global warming. *Geophys. Res. Lett.*, **37 (24)**, doi:10.1029/2010GL045440.

780 Ingram, W., 2012: A new way of quantifying GCM water vapour feedback. *Climate Dynam-*
781 *ics*, **Feb**, 10.1007/s00382-012-1294-3.

782 Jonko, A. K., K. M. Shell, B. M. Sanderson, and G. Danabasoglu, 2012: Climate feedbacks in
783 CCSM3 under changing CO₂ forcing. Part I: Adapting the linear radiative kernel technique
784 to feedback calculations for a broad range of forcings. *Journal of Climate*, doi:10.1175/
785 JCLI-D-11-00524.1.

786 Langen, P. L., R. G. Graversen, and T. Mauritsen, 2012: Separation of contributions from
787 radiative feedbacks to polar amplification on an aquaplanet. *Journal of Climate*, **25 (8)**,
788 3010–3024, doi:10.1175/JCLI-D-11-00246.1.

789 Myhre, G., E. J. Highwood, K. P. Shine, and F. Stordal, 1998: New estimates of radiative
790 forcing due to well mixed greenhouse gases. *Geophysical Research Letters*, **25** (14), 2715–
791 2718.

792 Pierrehumbert, R. T., 1995: Thermostats, radiator fins, and the local runaway greenhouse.
793 *Journal of the Atmospheric Sciences*, **52** (10), 1784–1806.

794 Ramaswamy, V., et al., 2001: Radiative forcing of climate change. *Climate Change 2001:*
795 *The Scientific Basis. Contribution of Working Group I to the Third Assessment Report of*
796 *the Intergovernmental Panel on Climate Change*, Houghton, J.T., Y. Ding, D.J. Griggs,
797 M. Noguer, P.J. van der Linden, X. Dai, K. Maskell, and C.A. Johnson, Ed., Cambridge
798 University Press, Cambridge, United Kingdom and New York, NY, USA, 881.

799 Randall, D., et al., 2007: Climate models and their evaluation. *Climate Change 2007: The*
800 *Physical Science Basis. Contribution of Working Group I to the Fourth Assessment Report*
801 *of the Intergovernmental Panel on Climate Change*, S. Solomon, D. Qin, M. Manning,
802 Z. Chen, M. Marquis, K. Averyt, M. Tignor, and H. Miller, Eds., Cambridge University
803 Press, Cambridge, United Kingdom and New York, NY, USA.

804 Roe, G. H. and K. C. Armour, 2011: How sensitive is climate sensitivity? *Geophys. Res.*
805 *Let.*, **38** (14), doi:10.1029/2011GL047913.

806 Roe, G., 2009: Feedbacks, timescales, and seeing red. *Annual Review of Earth and Planetary*
807 *Sciences*, **37**, 93–115.

808 Schlesinger, M. E., 1985: Feedback analysis of results from energy balance and radiative-
809 convective models. *The Potential Climatic Effects of Increasing Carbon Dioxide*, M. C.
810 MacCracken and F. M. Luther, Eds., U. S. Department of Energy, Washington, DC,
811 DOE/ER-0237, 280–319.

812 Senior, C. A. and J. F. B. Mitchell, 1993: Carbon dioxide and climate: The impact of cloud
813 parameterization. *Journal of Climate*, **6**, 393–418.

- 814 Senior, C. A. and J. F. B. Mitchell, 2000: The time dependence of climate sensitivity.
815 *Geophysical Research Letters*, **27 (17)**, 2685–2688, doi:10.1029/2000GL011373.
- 816 Shell, K. M., J. T. Kiehl, and C. A. Shields, 2008: Using the radiative kernel technique
817 to calculate climate feedbacks in NCAR’s Community Atmospheric Model. *Journal of*
818 *Climate*, **21 (10)**, 2269–2282, doi:10.1175/2007JCLI2044.1.
- 819 Shine, K. P., J. Cook, E. J. Highwood, and M. M. Joshi, 2003: An alternative to radiative
820 forcing for estimating the relative importance of climate change mechanisms. *Geophys.*
821 *Res. Lett.*, **30 (20)**, doi:10.1029/2003GL018141.
- 822 Shine, K. P. and P. M. Forster, 1999: The effect of human activity on radiative forcing of
823 climate change: a review of recent developments. *Global and Planetary Change*, **20 (4)**,
824 205 – 225, doi:10.1016/S0921-8181(99)00017-X.
- 825 Shine, K. P. and A. Sinha, 1991: Sensitivity of the earth’s climate to height-dependent
826 changes in the water vapour mixing ratio. *Nature*, **354 (6352)**, 382–384.
- 827 Soden, B. J., A. J. Broccoli, and R. S. Hemler, 2004: On the use of cloud forcing to estimate
828 cloud feedback. *Journal of Climate*, **17 (19)**, 3661–3665.
- 829 Soden, B. J., I. M. Held, R. Colman, K. M. Shell, J. T. Kiehl, and C. A. Shields, 2008:
830 Quantifying climate feedbacks using radiative kernels. *Journal of Climate*, **21 (14)**, 3504–
831 3520, doi:10.1175/2007JCLI2110.1.
- 832 Soden, B. J. and I. M. Held, 2006: An assessment of climate feedbacks in coupled ocean–
833 atmosphere models. *Journal of Climate*, **19 (14)**, 3354–3360, doi:10.1175/JCLI3799.1.
- 834 Soden, B. J. and G. A. Vecchi, 2011: The vertical distribution of cloud feedback in coupled
835 ocean-atmosphere models. *Geophysical Research Letters*, **38**, doi:10.1029/2011GL047632.
- 836 Solomon, S., et al., 2007: Technical Summary. *Climate Change 2007: The Physical Sci-*
837 *ence Basis. Contribution of Working Group I to the Fourth Assessment Report of the*

838 *Intergovernmental Panel on Climate Change*, S. Solomon, D. Qin, M. Manning, Z. Chen,
839 M. Marquis, K. Averyt, M. Tignor, and H. Miller, Eds., Cambridge University Press,
840 Cambridge, United Kingdom and New York, NY, USA.

841 Spencer, R. W. and W. D. Braswell, 1997: How dry is the tropical free troposphere? Implica-
842 tions for global warming theory. *Bulletin of the American Meteorological Society*, **78 (6)**.

843 Stephens, G. L., 2005: Cloud feedbacks in the climate system: A critical review. *Journal of*
844 *Climate*, **18 (2)**, 237–273, doi:10.1175/JCLI-3243.1.

845 Trenberth, K. E. and D. P. Stepaniak, 2003: Covariability of components of poleward at-
846 mospheric energy transports on seasonal and interannual timescales. *Journal of Climate*,
847 **16 (22)**, 3691–3705.

848 Tsushima, Y., et al., 2006: Importance of the mixed-phase cloud distribution in the control
849 climate for assessing the response of clouds to carbon dioxide increase: A multi-model
850 study. *Climate Dynamics*, **27**, 113–126, 10.1007/s00382-006-0127-7.

851 Watanabe, M., H. Shiogama, M. Yoshimori, T. Ogura, T. Yokohata, H. Okamoto,
852 S. Emori, and M. Kimoto, 2011: Fast and slow timescales in the tropical low-cloud re-
853 sponse to increasing CO₂ in two climate models. *Climate Dynamics*, 1–15, doi:10.1007/
854 s00382-011-1178-y.

855 Wetherald, R. T. and S. Manabe, 1988: Cloud feedback processes in a general circulation
856 model. *Journal of the Atmospheric Sciences*, **45 (8)**, 1397–1416.

857 Wyant, M. C., C. S. Bretherton, P. N. Blossey, and M. Khairoutdinov, 2012: Fast cloud
858 adjustment to increasing CO₂ in a superparameterized climate model. *Journal of Advances*
859 *in Modeling Earth Systems*, **4**.

860 Yoshimori, M., J. C. Hargreaves, J. D. Annan, T. Yokohata, and A. Abe-Ouchi, 2011:

861 Dependency of feedbacks on forcing and climate state in physics parameter ensembles.
862 *Journal of Climate*, **24**, 6440–6455, doi:10.1175/2011JCLI3954.1.

863 Zelinka, M. D. and D. L. Hartmann, 2012: Climate feedbacks and their implications for
864 poleward energy flux changes in a warming climate. *Journal of Climate*, **25**, doi:10.1175/
865 JCLI-D-11-00096.1.

866 Zelinka, M. D., S. A. Klein, and D. L. Hartmann, 2012: Computing and partitioning
867 cloud feedbacks using cloud property histograms. Part II: Attribution to changes in cloud
868 amount, altitude, and optical depth. *Journal of Climate*, doi:10.1175/JCLI-D-11-00249.1.

869 List of Tables

870 1 Global-mean, annual-mean feedbacks for fixed-SST (top row) and stratosphere-
871 adjusted (bottom row) radiative forcings. Planck (P), lapse rate (LR), water
872 vapor (WV), and albedo (A) feedbacks are unchanged as a function of forc-
873 ing. The “total feedback” is the sum of the linear feedbacks. We interpret
874 the residual as the nonlinear term. The terms in Equation 2 are normalized
875 by the global-mean surface temperature change, such that units are given in
876 $\text{W m}^{-2} \text{K}^{-1}$ unless otherwise noted.

38

Table 1: Global-mean, annual-mean feedbacks for fixed-SST (top row) and stratosphere-adjusted (bottom row) radiative forcings. Planck (P), lapse rate (LR), water vapor (WV), and albedo (A) feedbacks are unchanged as a function of forcing. The “total feedback” is the sum of the linear feedbacks. We interpret the residual as the nonlinear term. The terms in Equation 2 are normalized by the global-mean surface temperature change, such that units are given in $W\ m^{-2}\ K^{-1}$ unless otherwise noted.

Forcing ($W\ m^{-2}$)	Feedbacks							Total	Residual
	P	LR	WV	A	Net Cloud	LW Cloud	SW Cloud		
3.79	-3.03	-0.69	1.62	0.35	1.27	0.56	0.70	-0.49	-0.33
3.41	”	”	”	”	1.33	0.49	0.83	-0.43	-0.31

List of Figures

877

878

879

880

881

882

883

884

885

886

887

888

889

890

891

892

893

894

895

896

897

898

899

1 Zonal-mean, annual-mean T_s (top; K) and OLR (bottom; W m^{-2}) 10-year climatologies (gray) and anomalies (black). In both panels, solid gray lines indicate the $1\times\text{CO}_2$ climate; dashed lines, the $2\times\text{CO}_2$ climate. The global-mean equilibrium climate sensitivity is 4.69 K, though the meridional structure is strongly characterized by polar amplification. 42

2 (a) Zonal-mean radiative forcing (W m^{-2}) for CO_2 doubling: uniform 3.7 W m^{-2} (dashed gray) from Myhre et al. (1998), which serves as the basis for the IPCC Third Assessment Report estimates; stratosphere-adjusted forcing calculated from the GFDL radiative transfer code (solid gray, averaged over two months of $8\times$ daily model output); and fixed-SST forcing (solid black, averaged over 40 years), which includes rapid tropospheric adjustments. (b) LW (dotted) and SW (hashed) components of fixed-SST forcing. Net clear-sky stratosphere-adjusted forcing (solid gray) also shown for comparison to net clear-sky fixed-SST forcing (solid black). 43

3 Zonal-mean, annual-mean feedbacks ($\text{W m}^{-2} \text{ K}^{-1}$) for Planck (red), lapse rate (orange), water vapor (green), surface albedo (gray), cloud (blue), and the sum of these linear feedbacks (black). Thin lines represent feedbacks calculated with the stratosphere-adjusted, rather than fixed-SST, forcing. 44

4 (a) Zonal-mean, annual-mean shortwave (solid) and longwave (dashed) components of the cloud feedback ($\text{W m}^{-2} \text{ K}^{-1}$). (b) Change in cloud fraction. The zero contour is indicated by the heavy black line, and the contour interval is 2%; dark colors represent a decrease. 45

900 5 The balance of the three terms in Equation 2 (W m^{-2}). Recall that transport
 901 is the change in TOA net radiative flux, which in equilibrium must be equal to
 902 the change in convergence of atmospheric heat transport (i.e., $\Delta R = \Delta(\nabla \cdot F)$).
 903 The nonlinear term (black line) is calculated as the residual between merid-
 904 ional transport (dashed gray line) and the combined feedbacks and forcing
 905 (solid gray line). 46

906 6 (a) Zonal-mean, annual-mean partial temperature changes (K) attributed to
 907 forcing (red), nonlinear term (green), sum of non-Planck feedbacks (blue),
 908 and transport (black). The total surface temperature change is shown in
 909 gray. Components are weighted by the Planck feedback, which has meridional
 910 structure. (b) Local temperature change ΔT_s (K) if global-mean weighting
 911 $\overline{\lambda_P^{-1}}$ were instead applied in Equation 5 (dashed line). Solid line reproduced
 912 from gray line in upper panel. 47

913 7 Zonal-mean, annual-mean change in northward energy flux (PW). The total
 914 northward energy flux (thick gray) is obtained by integrating with respect
 915 to latitude the sum of the TOA and surface fluxes. The latent energy (solid
 916 black) is calculated from the integrated evaporation minus precipitation, and
 917 and the dry static energy (dashed black) is from the residual of the other two
 918 fluxes. 48

919 8 (a) Zonal-mean change in specific humidity (g kg^{-1}) averaged over 9 months
 920 (filled contours). Contour lines show streamlines for control climate. (b) Two
 921 estimates of the nonlinear term (W m^{-2}). Nonlinearity due to interactions
 922 amongst and within clear-sky feedbacks (solid), for the same time period as
 923 the top panel. Plotted for comparison is the residual nonlinearity (dashed) of
 924 Figure 5. 49

925 B1 Zonal-mean, annual-mean radiative kernels for the GFDL aquaplanet model.
926 (a) Temperature kernel and (b) water vapor kernel ($\text{W m}^{-2} \text{K}^{-1}$ per 100 hPa),
927 (c) surface albedo kernel ($\text{W m}^{-2} \text{K}^{-1}$ per %), and (d) surface temperature
928 kernel ($\text{W m}^{-2} \text{K}^{-1}$).

50

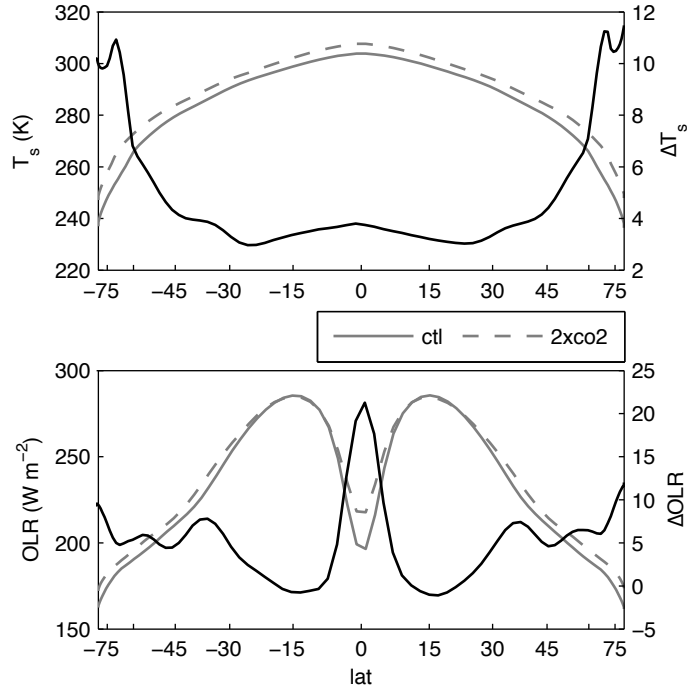


Figure 1: Zonal-mean, annual-mean T_s (top; K) and OLR (bottom; W m^{-2}) 10-year climatologies (gray) and anomalies (black). In both panels, solid gray lines indicate the $1\times\text{CO}_2$ climate; dashed lines, the $2\times\text{CO}_2$ climate. The global-mean equilibrium climate sensitivity is 4.69 K, though the meridional structure is strongly characterized by polar amplification.

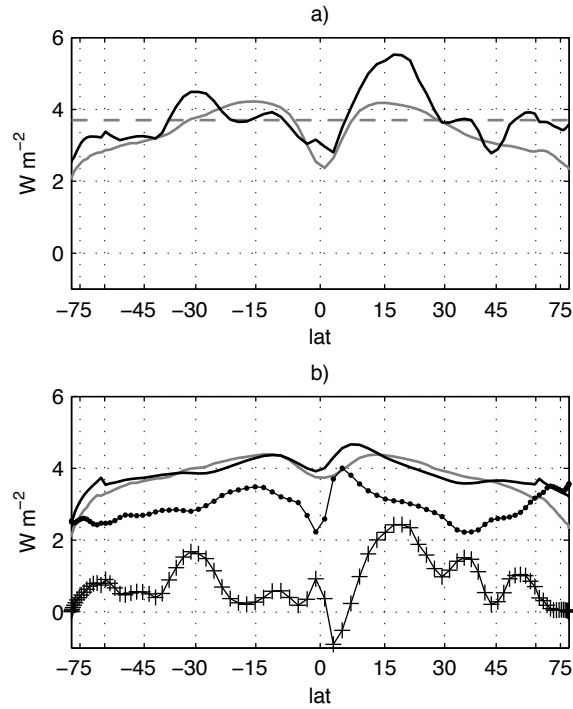


Figure 2: (a) Zonal-mean radiative forcing (W m^{-2}) for CO_2 doubling: uniform 3.7 W m^{-2} (dashed gray) from Myhre et al. (1998), which serves as the basis for the IPCC Third Assessment Report estimates; stratosphere-adjusted forcing calculated from the GFDL radiative transfer code (solid gray, averaged over two months of $8\times$ daily model output); and fixed-SST forcing (solid black, averaged over 40 years), which includes rapid tropospheric adjustments. (b) LW (dotted) and SW (hashed) components of fixed-SST forcing. Net clear-sky stratosphere-adjusted forcing (solid gray) also shown for comparison to net clear-sky fixed-SST forcing (solid black).

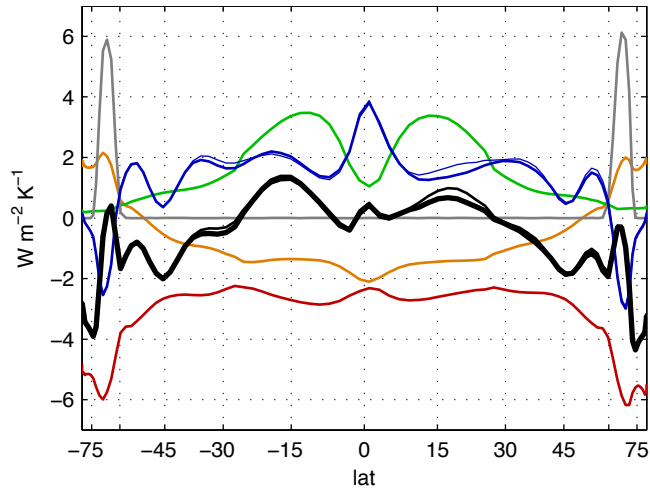


Figure 3: Zonal-mean, annual-mean feedbacks ($W m^{-2} K^{-1}$) for Planck (red), lapse rate (orange), water vapor (green), surface albedo (gray), cloud (blue), and the sum of these linear feedbacks (black). Thin lines represent feedbacks calculated with the stratosphere-adjusted, rather than fixed-SST, forcing.

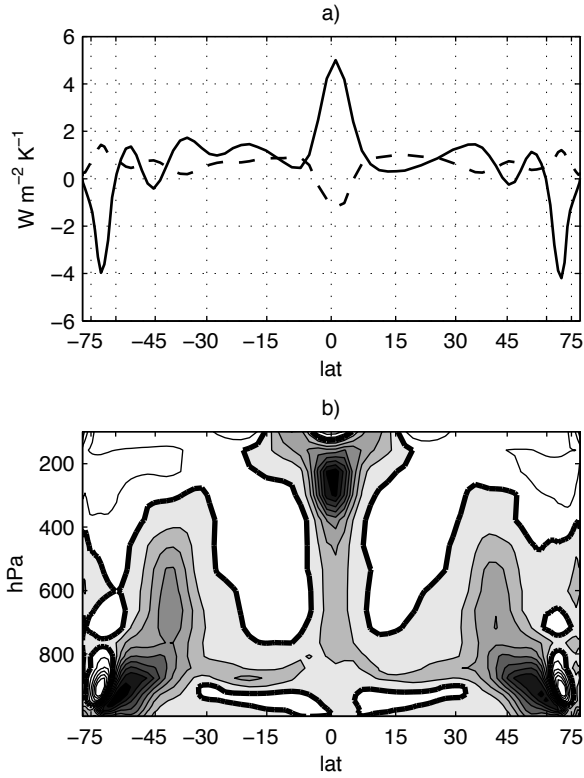


Figure 4: (a) Zonal-mean, annual-mean shortwave (solid) and longwave (dashed) components of the cloud feedback ($\text{W m}^{-2} \text{K}^{-1}$). (b) Change in cloud fraction. The zero contour is indicated by the heavy black line, and the contour interval is 2%; dark colors represent a decrease.

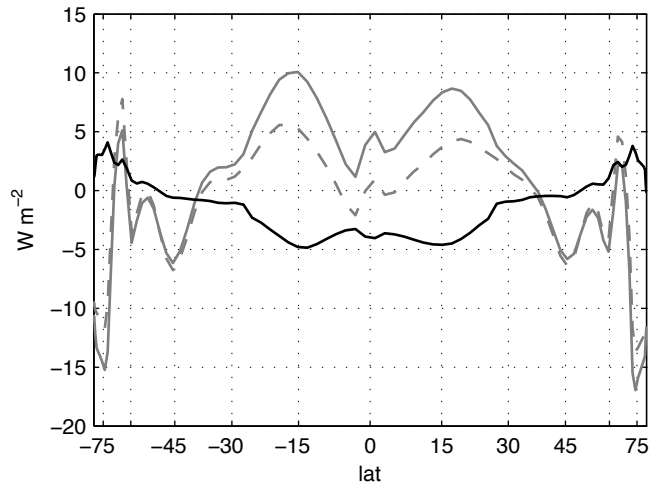


Figure 5: The balance of the three terms in Equation 2 (W m^{-2}). Recall that transport is the change in TOA net radiative flux, which in equilibrium must be equal to the change in convergence of atmospheric heat transport (i.e., $\Delta R = \Delta(\nabla \cdot F)$). The nonlinear term (black line) is calculated as the residual between meridional transport (dashed gray line) and the combined feedbacks and forcing (solid gray line).

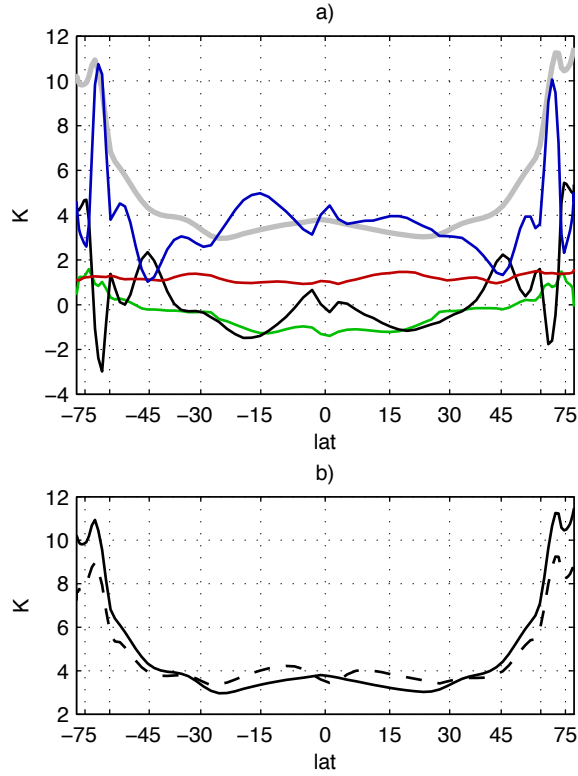


Figure 6: (a) Zonal-mean, annual-mean partial temperature changes (K) attributed to forcing (red), nonlinear term (green), sum of non-Planck feedbacks (blue), and transport (black). The total surface temperature change is shown in gray. Components are weighted by the Planck feedback, which has meridional structure. (b) Local temperature change ΔT_s (K) if global-mean weighting $\overline{\lambda_P^{-1}}$ were instead applied in Equation 5 (dashed line). Solid line reproduced from gray line in upper panel.

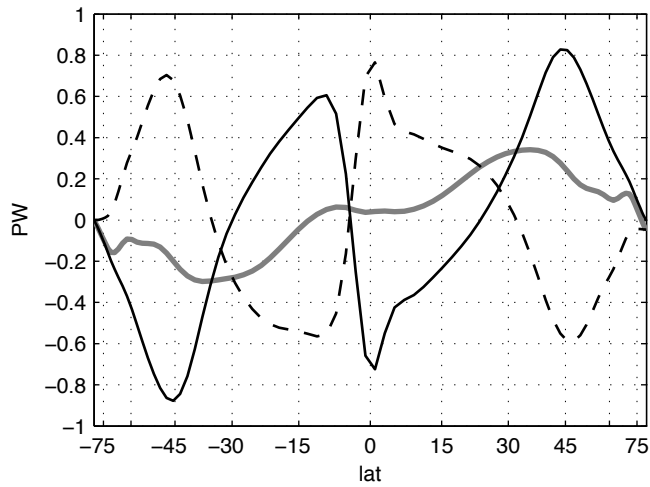


Figure 7: Zonal-mean, annual-mean change in northward energy flux (PW). The total northward energy flux (thick gray) is obtained by integrating with respect to latitude the sum of the TOA and surface fluxes. The latent energy (solid black) is calculated from the integrated evaporation minus precipitation, and the dry static energy (dashed black) is from the residual of the other two fluxes.

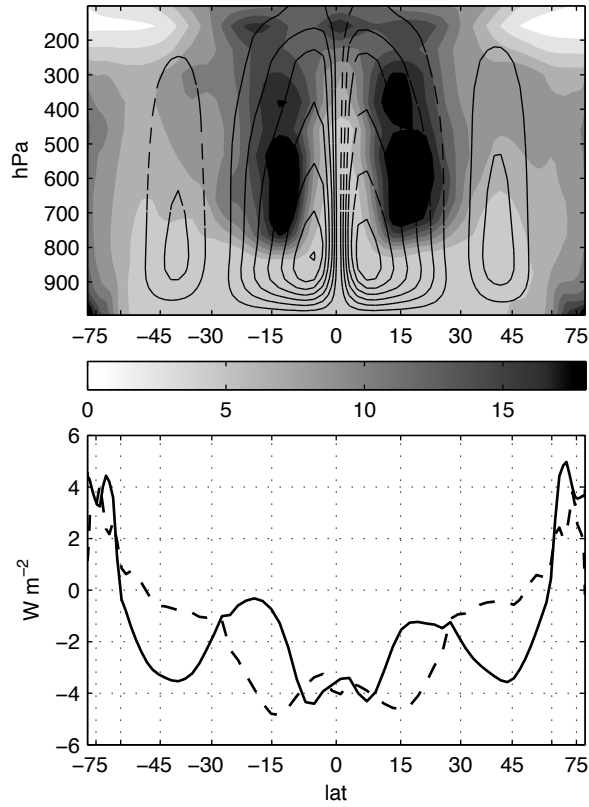


Figure 8: (a) Zonal-mean change in specific humidity (g kg^{-1}) averaged over 9 months (filled contours). Contour lines show streamlines for control climate. (b) Two estimates of the nonlinear term (W m^{-2}). Nonlinearity due to interactions amongst and within clear-sky feedbacks (solid), for the same time period as the top panel. Plotted for comparison is the residual nonlinearity (dashed) of Figure 5.

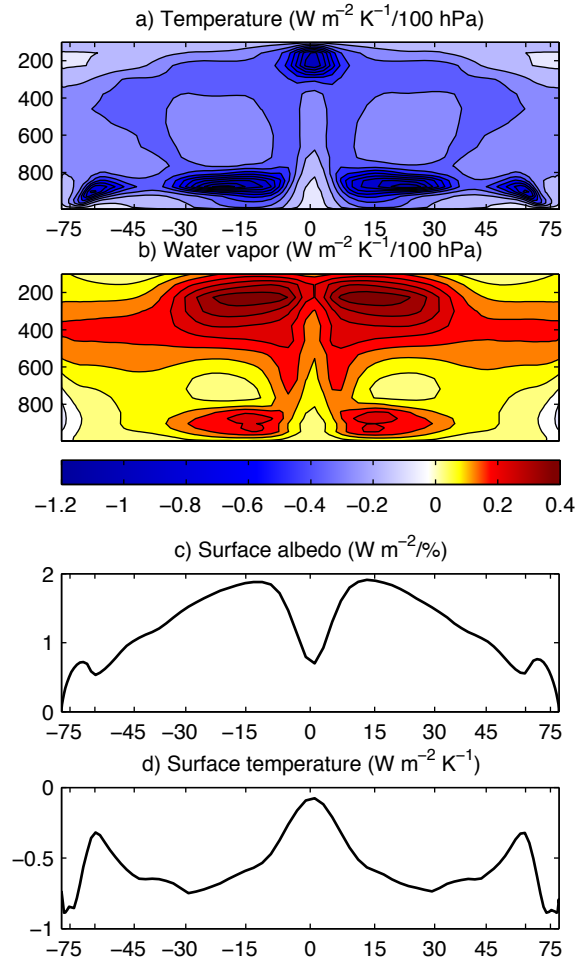


Figure B1: Zonal-mean, annual-mean radiative kernels for the GFDL aquaplanet model. (a) Temperature kernel and (b) water vapor kernel ($\text{W m}^{-2} \text{K}^{-1}$ per 100 hPa), (c) surface albedo kernel ($\text{W m}^{-2} \text{K}^{-1}$ per %), and (d) surface temperature kernel ($\text{W m}^{-2} \text{K}^{-1}$).